HHS Public Access

Author manuscript

Matrix Biol. Author manuscript; available in PMC 2024 January 01.

35kDa hyaluronan ameliorates ethanol driven loss of anti-microbial defense and intestinal barrier integrity in a TLR4-dependent manner

Semanti Ray[1,2], **Emily Huang**[1,2], **Gail A West**[1], **Marko Mrdjen**[1,3], **Megan R McMullen**[1,2], **Carol de la Motte**[1,4], **Laura E Nagy**[1,2,4]

[1]Department of Inflammation and Immunity, Cleveland Clinic, Cleveland, OH

[2]Northern Ohio Alcohol Center, Cleveland Clinic, Cleveland, OH

[3]Department of Cardiovascular and Metabolic Sciences, Cleveland Clinic, Cleveland, OH

[4]Department of Molecular Medicine, Case Western Reserve University, Cleveland, OH

Abstract

Acute and chronic alcohol exposure compromise intestinal epithelial integrity, due to reduced expression of anti-microbial peptides (AMP) and loss of tight junction integrity. Ameliorating gut damage is beneficial in preventing associated distant organ pathologies. Orally administered purified hyaluronan (HA) polymers with an average size of 35kDa have multiple protective effects in the gut and are well-tolerated in humans. Therefore, we tested the hypothesis that HA35 ameliorates ethanol-induced gut damage. Specifically, mechanisms that restore epithelial barrier integrity and normalize expression of the Reg3 class of C-type lectin AMPs (i.e. Reg3β and Reg3γ) were investigated. Chronic ethanol feeding to mice reduced expression of C-type lectin AMPs in the proximal small intestine (jejunum), reduced expression of tight junction proteins and increased bacterial translocation to the mesenteric lymph node. Oral consumption of HA35 during the last 6 days of ethanol exposure ameliorated the effects of chronic ethanol. Similarly, *in vitro* challenge of isolated intestinal organoids from murine jejunum with ethanol reduced the expression of C-type lectin AMPs and impaired barrier integrity; these ethanol-induced responses were prevented by pre-treatment with HA35. Importantly, HA receptor null jejunum-derived organoids demonstrated that the HA receptor *Tlr4*, but not *Cd44* nor *Tlr2*, was required for the protective effect of HA35. Consistent with the data from organoids, HA35 did not protect *Tlr4*-deficient mice from chronic ethanol-induced intestinal injury. Together, these data suggest therapeutic administration of HA35 is beneficial in restoring gut epithelial integrity and defense during the early stages of ethanol-driven intestinal damage.

Correspondence to Laura E Nagy: Department of Inflammation and Immunity, NE40, Cleveland Clinic, 9500 Euclid Ave, Cleveland, OH 44195. nagyl3@ccf.org.

Competing interests
None

Keywords

hyaluronan; alcohol; intestine; anti-microbial peptide; gut permeability; TLR4

Introduction

Chronic alcohol consumption impacts multiple organ systems and is associated with several chronic diseases, including liver disease, pancreatitis, lung injury, as well as increased susceptibility to bacterial and viral infections (1). There is growing appreciation that impaired functional integrity of the gastrointestinal tract is a critical target in the progression of alcohol-associated diseases. The impact of acute and chronic alcohol consumption on the intestinal organ system is manifold (2). Tight junction proteins, major regulators of epithelial barrier integrity and permeability, are down-regulated by ethanol (3). Chronic ethanol exposure causes microbial dysbiosis, including changes to bacterial, fungal, or viral communities (4–6). Loss of gut integrity is associated with increased leakage of endotoxin and other microbial metabolites into the portal circulation, exposing distal organs to microbial products, contributing to systemic inflammatory responses (3). Alcohol also reduces expression of small intestine resident anti-microbial peptides (AMPs), C-type lectin AMPs Reg3β and Reg3γ. Unlike the large intestine, the small intestine lacks mucus stratification; these AMPs are the main regulators of bacterial homeostasis and crucial in distancing the microbiome from invading the epithelial lining. Alcohol driven reduction in C-type lectin AMPs aggravates chronic liver disease (6).

Hyaluronan (HA), an extracellular-matrix component, exerts size, site and receptor-dependent effects. HA is recognized by, and signals through, multiple receptors, namely CD44, the receptor for HA-mediated motility (RHAMM), HA receptor for endocytosis (HARE), lymphatic vessel endothelial HA receptor (LYVE1), layilin, and toll-like receptors (TLRs), TLR2 and TLR4. Previous studies have determined that 35kDa sized fragments of HA (HA35) strengthen gut barrier function and resistance to bacterial infection (7). Mechanisms include up-regulation of the β-defensin AMPs in distal colon via TLR4 (8) and regulation of tight junction proteins in proximal colon via layilin (9). A clinical trial found that HA35 is well tolerated in humans (10) and an ongoing clinical trial is investigating HA35 as a therapeutic to mitigate the acute effects of alcohol on gut integrity (NCT05025865).

In the current study, we hypothesized that oral administration of HA35 would rescue ethanol-induced intestinal damage in proximal small intestine (jejunum) by modulation of AMP production and protection of epithelial barrier integrity. Using a murine model of chronic ethanol feeding and jejunum-derived organoids from C57BL/6J and *Tlr4*$^{-/-}$ mice, we report that HA35 normalizes ethanol-induced changes in gut integrity, expression of C-type lectin AMPs and bacterial translocation in C57BL/6J, but not *Tlr4*$^{-/-}$ mice.

Results and Discussion

Gut-targeted therapies have proven beneficial in not only protecting the gastrointestinal tract but also other organs from alcohol-associated injury. For instance, in murine models of

ALD, liver injury is reduced by restoring C-type lectin AMPs (11) or epithelial integrity (12). Therefore, it is essential to identify therapies that restore or maintain a healthy gut. We utilized a chronic ethanol feeding model in mice to induce intestinal damage. HA35 was administered in a voluntarily consumed jelly treat on the last 6 study days to mimic a therapeutic intervention (Fig S1). Differential expression of Reg3β and Reg3γ mRNA was observed. The highest expression was detected in the ileum, followed by jejunum and undetectable in the colon (Fig S2). Consequently, we focused on the small intestine for our study.

Chronic ethanol exposure reduced expression of mRNA (Fig 1A) and protein (Fig 1B) of both C-type lectin AMPs. HA35 treatment restored both AMPs in the jejunum but not in the ileum, therefore we focused our study on the jejunum (Fig 1A and B). The localized effect of HA35 could be attributed to variable receptor expression, presence of competing ligands, metabolic status of the cell or ligand-receptor affinity. Ethanol feeding reduced tight junction proteins, ZO-1 and occludin; expression was restored by HA35 treatment (Fig 1C). Ethanol also reduced the co-localization of ZO-1 and occludin in the jejunum and provision of HA35 maintained normal co-localization of these tight junction proteins (Fig 1D). Ethanol-induced perturbation of tight junctions was associated with loss of gut permeability assessed by increased fecal albumin levels. This was restored by HA35 supplementation (Fig 1E). Loss of both molecular (C-type lectin AMP) (13) and physical (tight junctions) (14) barriers in the gut enables bacterial migration across the epithelium. Ethanol feeding increased both aerobic and anaerobic colony forming units (CFU) in mesenteric lymph nodes (MLN), compared to pair-fed controls. The MLNs are the first organs encountered in bacterial translocation from the gastrointestinal tract into the systemic circulation. MLNs from HA35 treated ethanol-fed mice had fewer CFU (Fig 1F). Overall, these data demonstrate that HA35 restores multiple manifestations of ethanol-driven intestinal damage.

HA mediates its effects via interactions with individual receptors and/or a co-operative aggregation of multiple receptors (7). To identify the receptor involved in protecting the gut from chronic ethanol treatment, we utilized *in vitro* cultured intestinal epithelial organoids derived from jejunal crypts of mice deficient in the HA receptors TLR4, TLR2 and CD44. Traditional organoid culture methods produce organoids with the basolateral side exposed which may slow HA35 interaction with apical receptors. We reversed the polarity of organoids and cultured them apical out (15) to mimic the *in vivo* situation. Challenge of these organoids with ethanol reduced expression of C-type lectin AMPs in all genotypes. Pre-treatment with 200μg/ml HA35 prevented this reduction in C57BL/6J, *Cd44*$^{-/-}$ and *Tlr2*$^{-/-}$, but not in *Tlr4*$^{-/-}$ organoids (Fig 2A). *Tlr4*$^{-/-}$ organoids treated with HA35 alone showed reduced expression of AMP mRNAs; this might be attributed to activation of an inhibitory pathway upon HA35 binding to another HA receptor. In contrast, *Cd44*$^{-/-}$ organoids treated with HA35 trended towards higher mRNA expression of C-type lectin AMPs compared to the untreated organoids. This could be an effect of compensatory up-regulation of the other receptors of HA or the loss of an inhibitory mechanism downstream to CD44. Qualitative and quantitative assessment revealed that lack of *Tlr4* abolished the beneficial effect of HA35 on expression of C-type lectin AMPs, as well as restoration of epithelial barrier integrity (Fig 2B and 2C).

Since TLR4 mediated the effects of HA35 in murine organoids, we tested its role *in vivo*. Chronic ethanol feeding reduced expression of C-type lectin mRNA (Fig 3A) and protein (Fig 3B) in both C57BL/6J and *Tlr4*$^{-/-}$ mice. HA35 restored C-type lectin and tight junction protein expression in wild-type, but not *Tlr4*$^{-/-}$ mice (Fig 3B and 3C). Further, HA35 reduced fecal albumin content (Fig 3D) and plasma endotoxin in ethanol-fed C57BL/6J, but not *Tlr4*$^{-/-}$, mice (Fig 3E). Similarly HA35 failed to reduce CFU in MLN of ethanol-fed *Tlr4*$^{-/-}$ mice (Fig 3H) compared to the reduction in CFUs in C57B/6J mice.

Ethanol-driven impairments in gut integrity impact the pathophysiology of the liver, contributing to ethanol-induced liver injury. In the current model, ethanol increased hepatic triglyceride and expression of hepatic pro-inflammatory cytokine and chemokine mRNA (Fig S3 A/B). These responses were reduced by HA35. However, ethanol-induced induction of CYP2E1 and ER stress markers were unaffected by HA35 treatment (Fig S3 C), suggesting that HA35 does not protect from direct hepatotoxic effects of ethanol on the liver. In conclusion, using murine models of *in vivo* ethanol exposure and ethanol challenge to *in vitro* jejunal organoids we discovered that HA35 protects the proximal small intestine from ethanol driven loss of C-type lectin AMPs, epithelial integrity, and concomitant bacterial passage into MLN. Mechanistically, HA35 protects from ethanol-induced gut injury via TLR4 mediated mechanisms. This study sheds light on the possible use of HA35 as a therapeutic agent to prevent/treat early stages of alcohol-induced gastrointestinal injury.

Methods

Murine model of chronic ethanol feeding.

Eight- to ten-week-old C57BL6/J and *Tlr4*$^{-/-}$ (029015) mice were obtained from Jackson Laboratories (Bar Harbor, ME) and housed two per micro-isolator cage and acclimated to the Lieber-DeCarli liquid diet for 5 days. The Lieber-DeCarli high-fat liquid diet (#710260) was from Dyets, Bethlehem, PA. Highly purified, endotoxin-free Hyaluronan with a molecular weight distribution of 21–40kDa (HA35) (catalog # HA40K-1) was obtained from Life Core Biomedical (Chaska, MN). Ethanol was included in the liquid diet at a concentration of 5% v/v (28% of calories) for the last 10 days of the study. Maltose dextrin was isocalorically substituted in place of ethanol for pair-fed controls. During the last six days of the study, mice were provided with 15 mg/kg HA35 or an equivalent volume of water, as bolus contained in sterile jelly treats (composed of gelatin, stevia, and a flavoring agent, made in-house). Mice were trained with control jelly for 3 days, prior to HA35 treatment. Each mouse was given free access to one jelly. The morning after the last HA35 treatment, ethanol- and pair-fed mice were anesthetized, and samples collected post euthanasia. The intestine was excised and jejunum, ileum, proximal and distal colon were collected and fixed at room temperature in Histochoice (Amresco, Solon, OH) for 24 hours before paraffin blocking and sectioning. All animal procedures were approved and performed in accordance with the Institutional Animal Care and Use Committee at the Cleveland Clinic.

Mouse intestinal crypt isolation and culture.

The protocol for isolation of mouse intestinal crypts was modified from that reported by Miyoshi and Stappenbeck (16). The culture media was modified from Sato (17). Briefly, basal medium comprised of advanced DMEM F/12, 10% FBS, 5mM glutamine, 10mM HEPES, 1% penicillin/streptomycin. Additional growth factors including 100ng/ml Noggin (R&D, 1967/CF) 500ng/ml R-spondin 3-Fc conditioned media and 100ng/ml EGF-Fc conditioned media (Immunoprecise Antibodies, Utrecht, Netherlands) were added to the organoid growth media. Additionally, the Rho/ROCK inhibitor Y-27632 (10μM; Tocris, 1254) and ALK inhibitor A83–01 (1μM; Tocris, 2939) was also incorporated in the media. The final media was made fresh each time, before use. The cultures were incubated at 37°C in 5% CO_2 in air atmosphere in a humidified incubator for up to 3 days. Media was changed on the second day and organoids were passaged after 3 days of growth in matrigel domes.

Reversing polarity and differentiation of mouse intestinal organoids.

For experiments, pre-confluent spheroid cultures were taken (before spheroid centers appeared dark under phase contrast microscope visualization). The protocol for polarity reversal was adapted from Co *et.al.* (15) and modified. Briefly, 3–6 spheroid domes were scraped and suspended in 50mls of ice cold PBS containing 5mM EDTA. The solution was then kept rocking at 4°C for 1hr. Cells were collected by centrifuging (200g for 5 mins). The pellet was resuspended in 5mls of washing medium (DMEMF/12 containing 10% FBS, 1% penicillin/streptomycin and 1% L-glut) and centrifuged (200g for 5mins). The final pellet of apical-out organoids was resuspended in 1ml of differentiation media containing basal medium, growth factors, γ-secretase inhibitor DAPT (10μM; Tocris, 2634) and N-acetylcysteine amide (10μM; Sigma Aldrich, A0737). Organoids were cultured for 5 days, with half-media change every 2 days.

Permeability measurements of organoids treated with HA35 and ethanol.

Apical-out organoid cultures differentiated for 5 days were pre-treated with 200μg/ml HA35. After 24hrs, organoids were challenged with ethanol to a final concentration of 80mM for an additional 3hrs. The epithelial barrier integrity of organoids was measured by resistance to luminal accumulation of 40kDa FITC-Dextran. Briefly, after HA35 and ethanol treatment, organoids were kept on ice and the following steps were all carried out under cold conditions. Organoids were collected by centrifugation at 200g for 5mins, suspended in 1ml of Gentle Cell Dissociation Reagent (Stemcell Technologies, Canada) and incubated for 10mins at room temperature. Organoids were collected by centrifugation (200g for 5mins), suspended in 100μl of 1mg/ml 40kDa FITC-Dextran in PBS and incubated un-disturbed on ice for 5mins. After incubation, the supernatant was removed without disturbing the pellet. The pellet was suspended and loaded onto a glass slide for observation under 20X objective of a wide-field upright fluorescent microscope (Leica). Fluorescent and phase-contrast images were acquired for each organoid. Experiments were performed with organoids from 2–3 mice, and 20–30 organoids were imaged for each treatment condition.

Immunofluorescence of tight junctions in jejunum.

Frozen OCT sections of intestinal tissue was sectioned at 10um thickness. Primary antibodies were added including- occludin (1:100) (33–1500, Thermofisher Scientific, Waltham, MA) and ZO-1 (1:200) (61–7300, Invitrogen, Waltham, MA) for 30 mins at room temperature. Biotinylated anti-mouse IgG antibody was used followed by incubation with Streptavidin 488 (1:1000) and Alexafluor 548 donkey anti-rabbit (1:2000). TrueView Autofluoresence quenching (SP8500, Vector Laboratories, Burlingame, CA) was used before mounting slides with Vectashield Vibrance mounting media with DAPI (H-1800–10) (Vector Laboratories, Burlingame, CA). Images of jejunum were taken at 40X using Leica SP8 inverted confocal microscope. Maximum projection of z-stack images were used. Images are representative of 3 images per animal per condition.

Immunofluorescent staining of organoids.

The protocol for immunofluorescent staining of organoids was adapted from that reported by Co *et.al.*(15). Working solutions of primary antibodies against ZO-1 and Reg3β (1:100) and secondary antibodies (donkey anti-rabbit 633 (1:1000) and goat anti-rat 568 (1:1000) from Molecular Probes, Thermofisher Scientific, Waltham, MA) were prepared in the blocking solution (5% Bovine Serum Album, 3% Normal Goat Serum, 0.1% Triton X-100, 0.02% Tween 20 in 1X PBS). Images were acquired with Leica SP8 inverted microscope with a 40X objective (oil), zoom-1.0. Slides incubated without the primary antibody were used to correct for non-specific binding of the secondary antibodies. Positive staining for ZO-1 and Reg3β was quantitated by thresholding using ImageJ. The threshold cut-off was set using the control organoids and the signals from the treatment conditions were quantified using these threshold values. The acquired values were calculated over the DAPI signal for each organoid. 10–15 organoids were imaged per treatment condition.

Intestinal immunoblotting analysis.

Intestinal tissue sections were crushed with mortar-pestle in liquid nitrogen and collected in a lysis buffer (18) containing 8M urea, 1% SDS and 2.5M Tris (pH-7.5) with 1mM phenylmethanesulfonyl fluoride and Pierce Protease and Phosphatase Inhibitor (2 tablets/ 10ml). The solution was passed through a 21 gauge followed by 18 gauge needle and centrifuged at 13000rpm for 10mins. Supernatants were collected and diluted at 1:4 to perform the DC Lowry Protein Assay (Bio-Rad). Protein lysates were diluted to 1.5 mg/ml in Laemelli buffer (9), flash frozen in liquid nitrogen and stored at −80°C. Proteins were separated on 8 and 16% gels by SDS-PAGE and PVDF membranes were probed with antibodies against ZO-1 (1:1000), occludin (1:250), rat anti-Reg3β (R&D, MAB5110, 1:500) and rabbit anti-Reg3γ (Abcam, ab198216,1:1000) and then probed with respective secondary antibodies at 1:5000 dilution except for anti-guinea pig secondary antibody (1:2500). HSC-70 (mouse anti-HSC-70, Santa Cruz, sc-7298), was used as the loading control. Protein bands were visualized using ECL prime chemiluminescent development (GE Healthcare). Differences in chemiluminescent signal intensity were quantified using the ImageJ software (NIH Bethesda, MD, USA).

Liver immunoblotting analysis.

Frozen liver tissues (50–80mg) from mice were homogenized in lysis buffer (10ml/ g tissue) and protein concentration measured using the DC Lowry assay (Bio-Rad). Samples were prepared in Laemmli buffer and denatured at 97°C for 5 mins. Proteins were separated on 8 to 10% gels by SDS-PAGE and PVDF membranes were probed with antibodies against rabbit anti-Cyp2E1 (Abcam ab28146, 1:1000), rabbit anti-pEIF2α (Cell Signaling 3597, 1:1000) and rabbit anti-CHOP(Cell Signaling 5554, 1:1000). HSC-70 (mouse anti-HSC-70, Santa Cruz, sc-7298), was used as the loading control. Protein bands were visualized using ECL prime chemiluminescent development. Differences in chemiluminescent signal intensity were quantified using the ImageJ software.

Isolation of RNA and quantitative real-time polymerase chain reaction (qRT-PCR).

Total RNA was isolated from intestinal tissue and mouse intestine derived organoids using the Qiagen RNeasy Plus Universal Mini Kit (Cat. #74104) and RNeasy Micro Kit (Cat#74004) respectively, and reverse transcribed followed by amplification using qRT-PCR. 10μl of reaction mix contained cDNA, Power SYBR Buffer (ThermoFisher Scientific, Waltham, MA, USA) and primers at final concentrations of 1μM. qRT-PCR was performed in a Quantstudio 5 System for 40 cycles of 15 s at 95°C, 30 s at 60°C, 30 s at 72°C. The relative amount of target mRNA was determined using the comparative threshold (Ct) method by normalizing target mRNA Ct values to those of *18s*. Primer sequences are listed in Supplemental Table 1.

Bacterial cultures.

The protocol was adapted from Wang *et.al.*(13). At the time of mouse dissection, mesenteric lymph nodes were collected in a sterile fashion, homogenized using a Matrix D Lysis tube containing sterile thioglycolate media (BD, New Jersey, USA). 25μl culture was plated onto on REMEL Contact Agar plate (containing 5% sheep blood, ThermoFisher Scientific, Waltham, MA, USA) for culture of aerobic bacteria and 50μl on BBL Brucella Agar Plates (containing 5% horse blood) for culture of anaerobic bacteria. The plates were incubated for 72 hrs at 37°C under aerobic and anaerobic conditions respectively, followed by the counting of colony-forming units (CFUs).

Fecal Albumin ELISA.

Fecal albumin was determined by ELISA (Bethyl Labs) as described (5).

Biochemical assays.

Plasma samples were assayed for alanine aminotransferase (ALT) and aspartate aminotransferase (AST) using a commercially available enzymatic assay kit (Sekisui Diagnostics, Lexington, MA), following the manufacturer’s instructions. Total hepatic triglycerides were assayed using the Triglyceride Reagent Kit from Pointe Scientific Inc. (Lincoln Park, MI, USA). Plasma endotoxin concentrations were assayed by the Limulus Amebocyte Lysate Kinetic –QCL kit (Lonza, Walkersville, MD)

Statistical Analysis.

Differences between samples were assessed by ANOVA using the general linear model (SAS, Carey, IN). Multiple comparisons were analyzed using the least square means test. A significance threshold of $P<0.05$ was used to determine differences between comparisons. Values represent means ± SEM. Values with different alphabetical subscripts are significantly different. Sample size determination was performed by power calculations based on the primary outcome measures of hepatic TNF-α protein in mice after chronic ethanol indicate that 8 mice per group will be required to determine statistical significance of $p<0.05$ at 80% power. We expect to see a 60–85% change in expression; examples of means and SD from previous experiments were used in the power calculation. There is minimal unexpected loss of mice on this protocol, so we have not modified our power calculations to compensate for significant unexpected loss. Mice were randomly separated into groups, denoted by numbers and henceforth mice were referred to by codes for all experiments. The dotted line represents that statistical analysis was performed separately on the genotypes.

Supplementary Material

Refer to Web version on PubMed Central for supplementary material.

Acknowledgements

This work was supported in by NIH grant R01AA023764 and DOD grant PR190724 to LEN and CdlM. The authors thank the Imaging Core, Microbial Culture and Engineering Core and Biological Resources Unit at Lerner Research Institute. This work utilized the Leica SP8 confocal microscope that was purchased with funding from the National Institutes of Health Shared Instrumentation Grant 1S10OD019972-01.

Abbreviations:

HA	hyaluronan
HA35	35kDa sized hyaluronan
AMP	anti-microbial peptide
CFU	colony forming units
TLR	toll-like receptor
Reg3β	Regenerating islet derived protein 3 beta
Reg3γ	Regenerating islet derived protein 3 gamma
MLN	mesenteric lymph node
ALD	alcohol-associated liver disease

References

1. Patel S, Behara R, Swanson GR, Forsyth CB, Voigt RM, Keshavarzian A. Alcohol and the Intestine. Biomolecules. 2015;5(4):2573–88. [PubMed: 26501334]
2. Bishehsari F, Magno E, Swanson G, Desai V, Voigt RM, Forsyth CB, et al. Alcohol and Gut-Derived Inflammation. Alcohol Res. 2017;38(2):163–71. [PubMed: 28988571]

3. Khair S, Brenner LA, Koval M, Samuelson D, Cucinello-Regland JA, Anton P, et al. New insights into the mechanism of alcohol-mediated organ damage via its impact on immunity, metabolism, and repair pathways: A Summary of the 2021 Alcohol and Immunology Research Interest Group (AIRIG) meeting. Alcohol. 2022.
4. Duan Y, Llorente C, Lang S, Brandl K, Chu H, Jiang L, et al. Bacteriophage targeting of gut bacterium attenuates alcoholic liver disease. Nature. 2019;575(7783):505–11. [PubMed: 31723265]
5. Hartmann P, Chen P, Wang HJ, Wang L, McCole DF, Brandl K, et al. Deficiency of intestinal mucin-2 ameliorates experimental alcoholic liver disease in mice. Hepatology. 2013;58(1):108–19. [PubMed: 23408358]
6. Hendrikx T, Schnabl B. Antimicrobial proteins: intestinal guards to protect against liver disease. J Gastroenterol. 2019;54(3):209–17. [PubMed: 30392013]
7. Kim Y, de la Motte CA. The Role of Hyaluronan Treatment in Intestinal Innate Host Defense. Front Immunol. 2020;11:569. [PubMed: 32411124]
8. Hill DR, Kessler SP, Rho HK, Cowman MK, de la Motte CA. Specific-sized hyaluronan fragments promote expression of human beta-defensin 2 in intestinal epithelium. J Biol Chem. 2012;287(36):30610–24. [PubMed: 22761444]
9. Bellos DA, Sharma D, McMullen MR, Wat J, Saikia P, de la Motte CA, et al. Specifically Sized Hyaluronan (35 kDa) Prevents Ethanol-Induced Disruption of Epithelial Tight Junctions Through a layilin-Dependent Mechanism in Caco-2 Cells. Alcohol Clin Exp Res. 2019;43(9):1848–58. [PubMed: 31237689]
10. Bellar A, Kessler SP, Obery DR, Sangwan N, Welch N, Nagy LE, et al. Safety of Hyaluronan 35 in Healthy Human Subjects: A Pilot Study. Nutrients. 2019;11(5).
11. Yan AW, Fouts DE, Brandl J, Starkel P, Torralba M, Schott E, et al. Enteric dysbiosis associated with a mouse model of alcoholic liver disease. Hepatology. 2011;53(1):96–105. [PubMed: 21254165]
12. Kirpich IA, Feng W, Wang Y, Liu Y, Barker DF, Barve SS, et al. The type of dietary fat modulates intestinal tight junction integrity, gut permeability, and hepatic toll-like receptor expression in a mouse model of alcoholic liver disease. Alcohol Clin Exp Res. 2012;36(5):835–46. [PubMed: 22150547]
13. Wang L, Fouts DE, Starkel P, Hartmann P, Chen P, Llorente C, et al. Intestinal REG3 Lectins Protect against Alcoholic Steatohepatitis by Reducing Mucosa-Associated Microbiota and Preventing Bacterial Translocation. Cell Host Microbe. 2016;19(2):227–39. [PubMed: 26867181]
14. Schnabl B, Brenner DA. Interactions between the intestinal microbiome and liver diseases. Gastroenterology. 2014;146(6):1513–24. [PubMed: 24440671]
15. Co JY, Margalef-Catala M, Monack DM, Amieva MR. Controlling the polarity of human gastrointestinal organoids to investigate epithelial biology and infectious diseases. Nat Protoc. 2021;16(11):5171–92. [PubMed: 34663962]
16. Miyoshi H, Stappenbeck TS. In vitro expansion and genetic modification of gastrointestinal stem cells in spheroid culture. Nat Protoc. 2013;8(12):2471–82. [PubMed: 24232249]
17. Sato T, Vries RG, Snippert HJ, van de Wetering M, Barker N, Stange DE, et al. Single Lgr5 stem cells build crypt-villus structures in vitro without a mesenchymal niche. Nature. 2009;459(7244):262–5. [PubMed: 19329995]
18. Cash HL, Whitham CV, Behrendt CL, Hooper LV. Symbiotic bacteria direct expression of an intestinal bactericidal lectin. Science. 2006;313(5790):1126–30. [PubMed: 16931762]

HIGHLIGHTS

1. Our study identifies a novel, beneficial role of purified hyaluronan (HA) polymers with an average size of 35kDa (HA35) in ameliorating ethanol-driven injury in the gastrointestinal tract. 2. Using both in vivo mouse model of chronic ethanol feeding and in vitro ethanol-challenge of murine jejunal organoids we demonstrate that treatment with HA35 normalizes all aspects of ethanol-driven gut injury namely, loss of C-type lectin anti-microbial peptides, loss of intestinal integrity and bacterial translocation to the mesenteric lymph node. 3. We identify the proximal small intestine (jejunum) as a new site of HA35 mediated gut-protection. 4. We also identify a novel role of hyaluronan in regulating the C-type lectin class of the anti-microbial peptides, via its receptor, TLR4. 5. We have utilized intestinal organoids from multiple hyaluronan receptor-null mice strains and an in vivo chronic ethanol feeding in Tlr4-null mice to show that the hyaluronan receptor Tlr4 is essential for the protective effects of HA35 in the gut. 6. Our study sheds light on the potential use of HA35 as a therapeutic agent to prevent/treat early stages of alcohol-induced gastrointestinal injury.

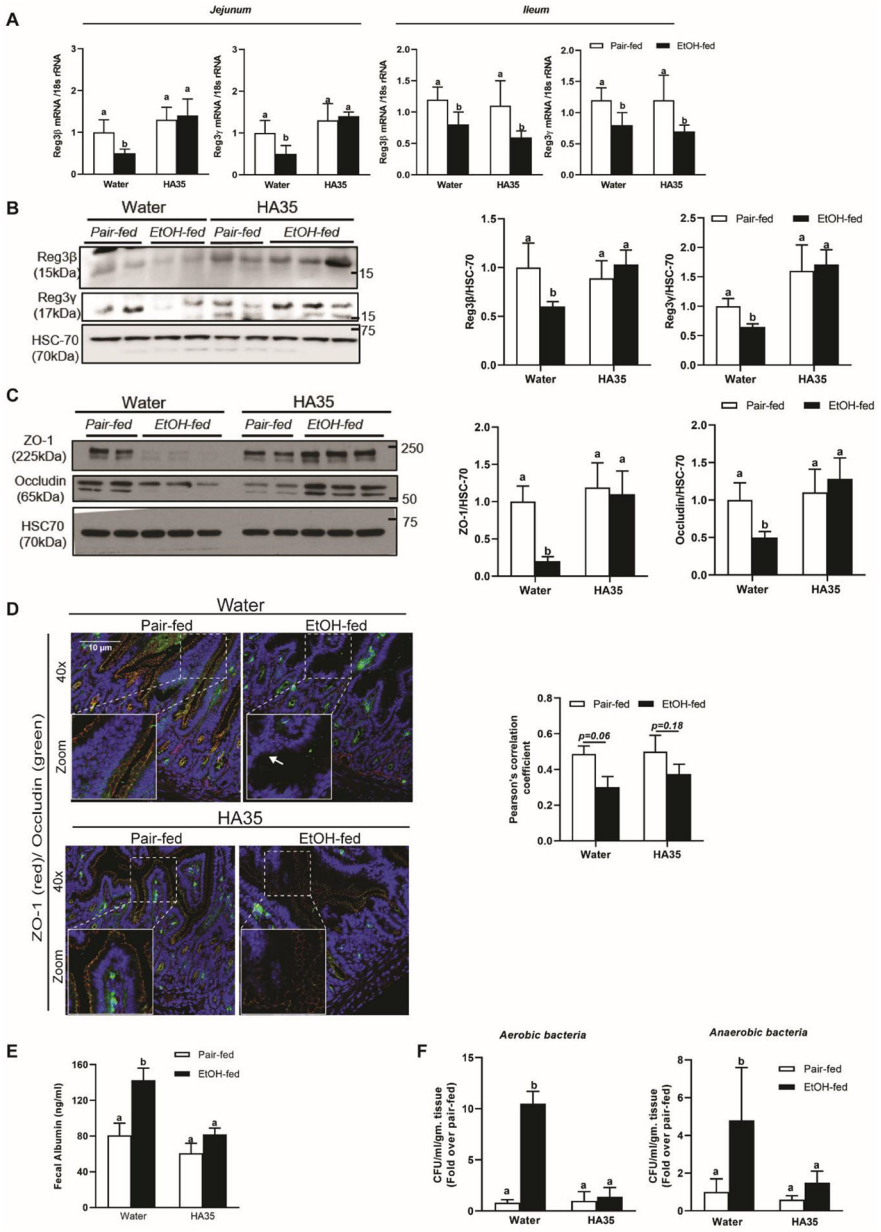

Figure 1: HA35 abrogates ethanol induced reduction of C-type lectin AMPs, tight junction proteins ZO-1 and occludin and bacterial translocation, in the proximal small intestine.

C57BL/6J male mice exposed to chronic ethanol feeding were administered 15mg/kg HA35 on the last 6 days of the study. **(A)** Expression of Reg3β and Reg3γ mRNA in Jejunum and Ileum was quantified using quantitative real-time PCR (qRT-PCR) and normalized to 18S rRNA. *N*= 8–12 mice per group. Protein expression of jejunum associated **(B)** Reg3β (15kDa) and Reg3γ (17kDa) **(C)** ZO-1 (190–225kDa) and occludin (65kDa) was assessed by Western blot analysis and normalized to HSC70. **(D)** Immunofluorescence staining and quantification of tight junction proteins, ZO-1 and occludin from histochoice-preserved paraffin-embedded sections of jejunum. Confocal microscopic images were acquired at 40X magnification and are representative of *N*= 4–6 mice per group. **(E)** Fecal Albumin concentration. **(F)** Bacterial translocation to the mesenteric lymph node graphed as fold

change over pair-fed control. $N = 8–12$ mice per group. P less than 0.05, assessed by 2-way ANOVA; values with different alphabetical superscripts are significantly different from each other.

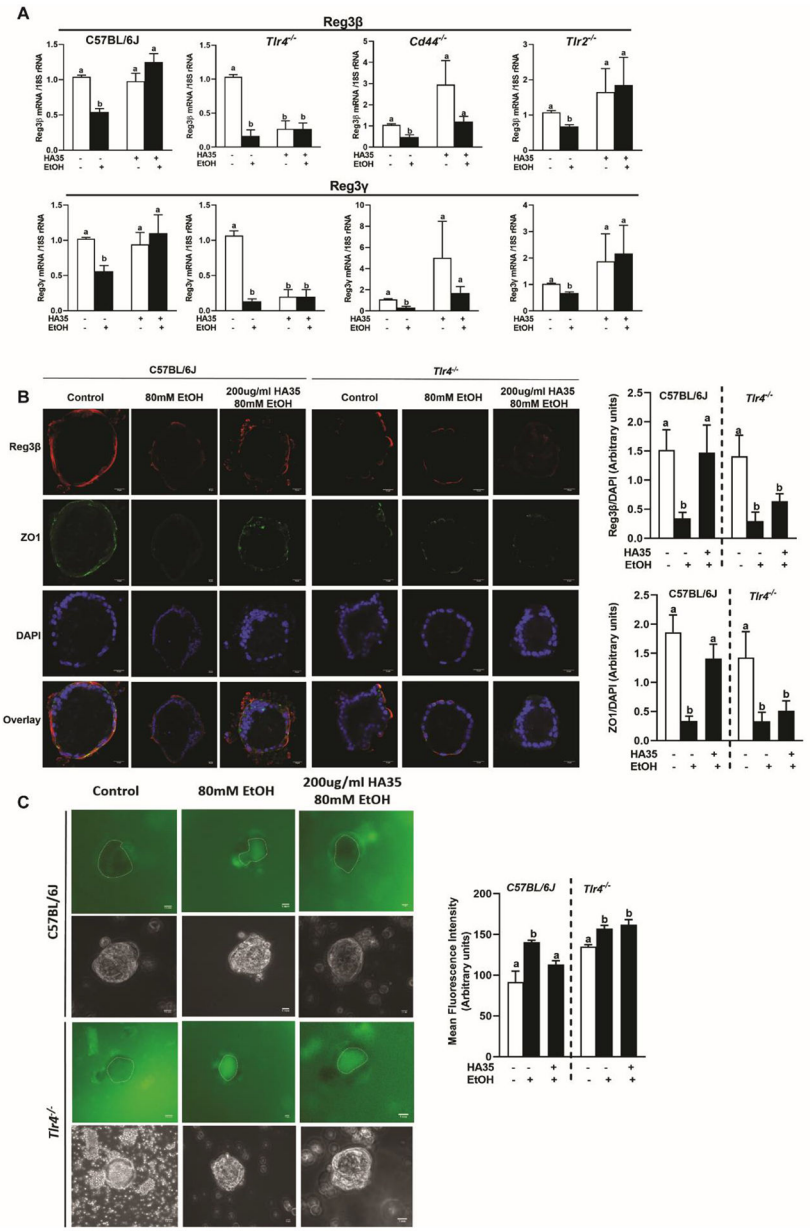

Figure 2: The cell surface receptor TLR4 is essential for HA35 mediated rescue of C-type lectin AMPs, tight junction protein ZO-1 and maintenance of epithelial integrity in ethanol-challenged mice jejunum-derived organoids.

Jejunum-derived organoids from C57BL/6J, *Tlr4*$^{-/-}$, *Cd44*$^{-/-}$, *Tlr2*$^{-/-}$ male mice were differentiated to grow apical out, pre-treated with 200μg/ml HA35 for 24hrs followed by ethanol challenge 3hrs. **(A)** Expression of Reg3β and Reg3γ mRNA was detected using quantitative real-time PCR (qRT-PCR) and normalized to 18S rRNA. Experiments were repeated at least thrice with 2–3 technical replicates per experiments and $N = 4$ biological replicates per group. **(B)** Immunofluorescence staining of Reg3β and ZO-1 in C57BL/6J and *Tlr4*$^{-/-}$ differentiated apical out organoids. Images were acquired at 40X magnification and are representative of $N = 10–15$ organoids per condition. All treatment conditions of a genotype were normalized to the untreated control of the same genotype. **(C)** Epithelial

integrity was quantitatively analyzed in jejunum organoids by estimating the luminal accumulation of 40kDa FITC-Dextran. A broken line is used to demarcate the luminal periphery. Images were acquired at 20X magnification and are representative of *N*= 20–30 organoids per treatment group. All treatment conditions were normalized to the untreated control of the same genotype. P less than 0.05, assessed by 2-way ANOVA; values with different alphabetical superscripts are significantly different from each other.

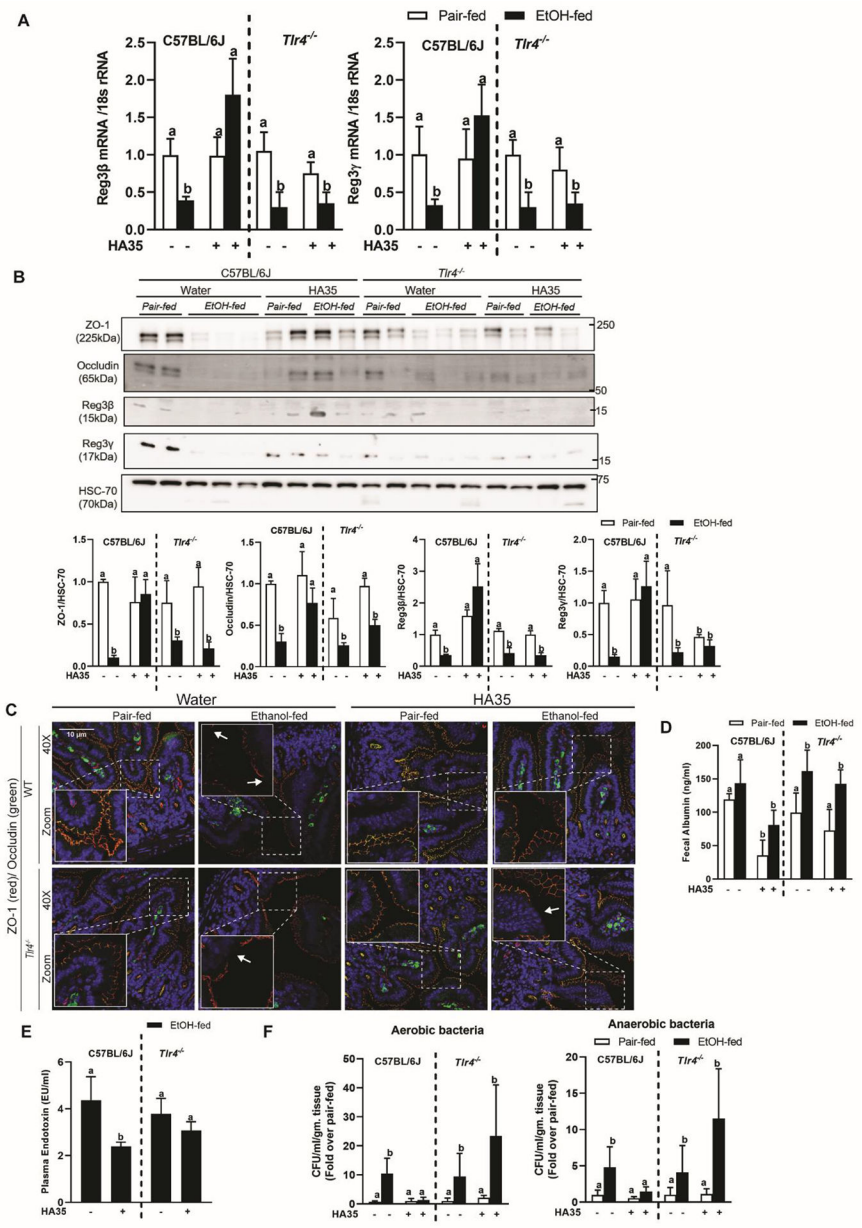

Figure 3: Tlr4 deletion abrogates HA35 mediated amelioration of ethanol-induced loss of epithelial barrier defense and integrity, in the proximal small intestine.

C57BL/6J and *Tlr4*$^{-/-}$ mice were put on the regimen of chronic ethanol feeding and HA35 treatment. **(A)** Expression of Reg3β and Reg3γ mRNA in jejunum was quantified using quantitative real-time PCR (qRT-PCR) and normalized to 18S rRNA. *N*= 8–12 mice per group. **(B)** Western blotting was used to assay protein expression of C-type lectin AMPs, Reg3β and Reg3γ, and tight junction proteins, ZO-1 and occludin from jejunal lysates. HSC-70 was used as the loading control. **(C)** Immunofluorescence staining of tight junction proteins, ZO-1 and occludin from histochoice-preserved paraffin-embedded sections of jejunum. Images are representative of *N*= 4–6 mice per group. **(D)** Fecal albumin concentration**. (E)** Plasma endotoxin concentration**. (F)** Bacterial colonies detected in mesenteric lymph nodes normalized to fold change over genotype pair-fed control. *N*=

8–12 mice per group P less than 0.05, assessed by 2-way ANOVA; values with different alphabetical superscripts are significantly different from each other.